Bulletin of the Seismological Society of America, Vol. 101, No. 1, pp. 385–398, February 2011, doi: 10.1785/0120100029

The Effects of Double Fault Bends on Rupture Propagation: A Geometrical Parameter Study

by Julian C. Lozos, David D. Oglesby, Benchun Duan, and Steven G. Wesnousky

Abstract We use the 2D finite element method to determine how geometrical parameters determine whether rupture will propagate across a linked stepover in a strike-slip fault. The end segments of the fault system are aligned in the direction of maximum shear, and the length and angle of the linking segment are allowed to vary. We observe that ruptures propagate through extensional stepovers with steeper angles and longer linking segments than otherwise equivalent compressional stepovers. These different rupture behaviors form distinct regions in angle-stepover-length parameter space; the boundary between these regions takes the shape of an asymptotic curve in both the extensional and compressional cases. Models in which the size of the entire fault system was made larger or smaller revealed that the location of the boundaries between regions of different rupture behavior do not scale linearly with the system size; it was easier to rupture steeper and relatively longer stepovers in fault systems that were larger overall. A separate set of models in which the stress field is rotated so that the parallel end segments were optimally aligned for rupture significantly altered the rupture behavior curves; in this stress field, it was easier to rupture compressional stepovers with steeper angles and longer linking segments than it was to rupture equivalent extensional stepovers. In both the case in which the end segments are aligned with the direction of maximum shear and the case in which the end segments are optimally oriented for rupture, the angles at which rupture could no longer propagate through the entire fault corresponded with peaks in the fault's S value.

Introduction

Segmented faults with stepovers are ubiquitous in nature. They occur on a wide range of scales (Segall and Pollard, 1980); for example, in southern California, they range from small stepovers on the San Jacinto fault to the large-scale stepover on the San Andreas fault between Tejon Pass and San Gorgonio Pass. Because this type of fault geometry is so prevalent, nonplanar fault geometry must be considered in the analysis of seismic hazard. In particular, the dynamics of fault systems with linked stepovers are different from the dynamics of planar faults, as each segment interacts differently with the ambient stress field depending on its orientation and as dynamic effects can lead to both compression and dilation in the stepover region. The compressional case and the extensional case are also quite different from each other, as dynamic unclamping makes the linking segment in the extensional case more favorable for rupture, whereas clamping makes the linking segment in a compressional system more difficult to rupture (Oglesby, 2005); our present results are more complicated than this basic result. Understanding how these factors affect rupture behavior and propagation is important for addressing the issue of what factors make rupture stop, which can in turn be applied to determination of rupture length and expected magnitudes. In the 2D models in this study, we modeled fault systems consisting of two parallel strike-slip segments linked by a segment on which motion is constrained to be strike slip, over a wide range of bend angles and stepover lengths, at several different overall system scales, and in two different regional stress fields. Our overall aim was to determine the range of bend angles and stepover lengths that allow or prevent through-going rupture propagation and thus larger earthquakes.

Understanding how complexities in fault geometry affect rupture behavior is one of many aspects in understanding what makes earthquake rupture stop. Wesnousky (2008) examined 37 large historic earthquakes with mapped surface ruptures (most of which were strike slip) and found that about two-thirds of these ruptures terminated at geometrical discontinuities along the mapped fault trace. Isolating different types of geometrical complexities and parameterizing their effects on rupture behavior will be useful in evaluating potential endpoints of future ruptures on large faults. This process may allow for some estimation of eventual earthquake size,

which in turn might allow for better assessment of seismic hazard associated with a particular fault.

A significant body of work already exists concerning the behavior of nonplanar faults (e.g., Harris *et al.*, 1991; Aochi *et al.*, 2000; Anderson *et al.*, 2003; Kame *et al.*, 2003; Oglesby *et al.*, 2003; Duan and Oglesby, 2005, 2007; Oglesby, 2008). In particular, there have been several previous studies concerning dynamic rupture on faults with stepovers. Harris and Day (1993) performed a benchmark study on the dynamics of parallel strike-slip faults with disconnected stepovers. They modeled a system consisting of two fault segments separated by some variable distance, in order to determine at which distance rupture no longer jumped from segment to segment, in both compressional and extensional cases. They found that rupture can jump from segment to segment in both extensional and compressional cases, though the jumpable distance is longer in extensional stepovers than in compressional ones, and that the actual jumpable distance depended on model parameters related to rupture velocity.

The problem of an unlinked stepover is somewhat different from a linked one, however. Rupture propagates more easily through linked stepovers than unlinked ones because rupture can continue through all segments of the fault without stopping. Unlinked stepovers require that stress changes induced by seismic waves renucleate rupture on the secondary fault strand, as shown by Magistrale and Day (1999), who focused on determining the width of stepover through which rupture could propagate along thrust fault systems. Their study tested cases with and without a linking fault segment. They found unambiguously that the presence of a linking fault segment greatly increases the stepover width through which rupture can propagate. In a related study, Oglesby (2005) examined the dynamics of parallel strike-slip faults with dip-slip linking segments. He compared these types of systems to strike-slip systems without any type of linking fault, and also examined whether rupture propagation is affected by whether nucleation occurs on the dip-slip linking segment or one of the parallel strike-slip segments. He found that the presence of a linking dip-slip fault makes it easier for rupture to propagate through a stepover between strike-slip faults in general, and that extensional strike-slip systems with linking normal faults are more susceptible to longer rupture than compressional systems with linking thrust faults. Unlike these past works, the present study examines the dynamics of faults with parallel strike-slip segments joined by a strike-slip linking segment. The computational efficiency of a 2D method allows us to make a thorough parameterization of rupture behavior over a given range of stepover angles and linking segment lengths for both extensional and compressional cases. Thus, we may investigate quantitatively the limits of rupture's ability to propagate through stepovers. We also examine the effects of the overall fault system size and the orientation of the regional stress field on rupture behavior.

Method

Our model geometry is of a simplified linked stepover on a strike-slip fault (Fig. 1). It consists of two parallel end segments (the left is referred to as the nucleating segment throughout this paper; the right is referred to as the far segment) of a set length connected at a variable angle by a linking segment of variable length. The size of the linking segment is denoted as its actual length, rather than the perpendicular distance between the nucleating segment and the end segment. We simulated fault systems with linking fault angles up to 45°. Switching the direction of the shear stress field allowed the modeling of both compressional and extensional stepovers. Most of our models were conducted with a regional stress field such that the main segments were aligned with the direction of maximum shear stress; however, we also tested models in which the main segments were at the most favorable orientation for rupture, as determined by minimizing the difference between the fault's yield stress and initial shear stress. All ruptures were artificially nucleated on the left-most parallel segment by forcing rupture to proceed outward at a fixed speed until the critical patch size for spontaneous rupture propagation was reached (Day, 1982).

The dynamic rupture models were performed using the 2D finite element code EQdyna2d (Duan and Oglesby, 2006). We used Coulomb friction ($\tau \leq \mu\sigma_n$, where τ is frictional stress, μ is the coefficient of friction, and σ_n is the normal stress) and a slip-weakening friction law in which the fault's coefficient of friction drops from its static value to its sliding value over a specified distance (Ida, 1972; Palmer and Rice, 1973; Andrews, 1976a). Our models assume elastic behavior off the fault. Our physical and computational parameters are listed in Table 1.

Our 2D approximation and the numerical efficiency of EQdyna2D allowed us to run a large enough number of models, producing a thorough exploration of parameter space for rupture behaviors on linked stepovers over a wide range of stepover lengths and angles.

We performed three sets of faulting models. The first set, referred to hereafter as the basic case, is a full parameterization of transitions between different rupture behaviors on extensional and compressional stepovers with parallel segments fixed at 10 km in length, and a linking segment

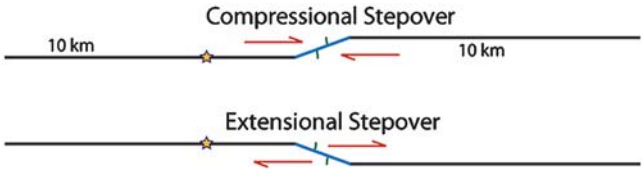

Figure 1. Diagram of fault geometry. The blue line represents the linking segment, which is variable in length. The green arcs show the stepover angle, taken relative to the strike of the parallel end segments; this angle is also variable. The red arrows represent the direction of slip. The star marks the nucleation point, 7 km along the nucleating segment of the fault. The lengths of the nucleating and far segments, in black, are constant at 10 km each.

Table 1
Physical and Computational Parameters

P-wave velocity	6000 m/s
S-wave velocity	3464 m/s
Density	2700 kg/m^3
Static frictional coefficient	0.6
Sliding frictional coefficient	0.3
Slip-weakening parameter	0.2 m
Normal stress on parallel end segments	−100 MPa
Shear stress on parallel end segments	45 MPa
Element size	10 m
Size of nucleation zone	500 m

ranging between 500 m and 8 km in length. In the second set, the entire fault system was made larger or smaller to test how rupture behavior scaled with fault system size. There were two subsets to this series of models: one with the nucleation point a fixed distance of 3 km from the stepover, and the other with the nucleation distance from the stepover scaled relative to the size of the entire system. We made this distinction to account for any possible effects of rupture velocity on behavior. Rupture velocity should approach the Rayleigh wave speed, but if the rupture front is given enough space, it may jump to supershear velocity (Andrews, 1976b). Our choice of a nucleation point at 3 km from the first bend allows the rupture front to reach at least Rayleigh speed in all cases. Thus, increasing the amount of space between the nucleation point and the first bend, as in the cases where the overall size of the whole fault system was increased, might allow for the rupture front to reach supershear velocity before reaching the bend, changing the rupture behavior. Similarly, in the systems that were smaller overall, the rupture front may not reach Rayleigh velocity by the time it approaches the first bend, which also has an effect on how the rupture front negotiates the bend. The third set of models (hereafter referred to as the stress rotation case) kept the same geometry as the first set, but had a stress field such that the parallel end segments were optimally aligned for rupture, as opposed to aligned parallel with the direction of maximum shear as in the basic case. The differences between the regional stress field in the basic case and in the stress rotation case are illustrated in Figure 2.

Results

Basic Case

Our starting test case consisted of a fault with parallel end segments fixed at 10 km each, with a nucleation point fixed at 3 km from the right corner of the nucleating segment (7 km from the left edge of the fault system). The stress field was such that the parallel end segments were in line with the direction of maximum shear stress. We modeled this system with a wide range of stepover lengths and connecting angles as both extensional and compressional cases, in order to determine at which lengths and which angles did the rupture no longer proceed through all three segments of the fault.

We observed five distinct rupture behaviors:

1. Figure 3a shows graphs of rupture on a 35°-extensional stepover with a 2 km linking segment at several timesteps. In each graph, the first panel shows the stresses along the fault's strike, with yield stress in red and shear stress in blue. The linking segment is evident by the difference in initial stresses; these differences are imposed by the constant regional stress field interacting differently with the strike of this segment relative to the strike of the parallel end segments. The second panel shows slip velocity at all points along strike, and the third panel shows cumulative slip at all points along strike. In this particular case, the first graph shows bilateral rupture propagation

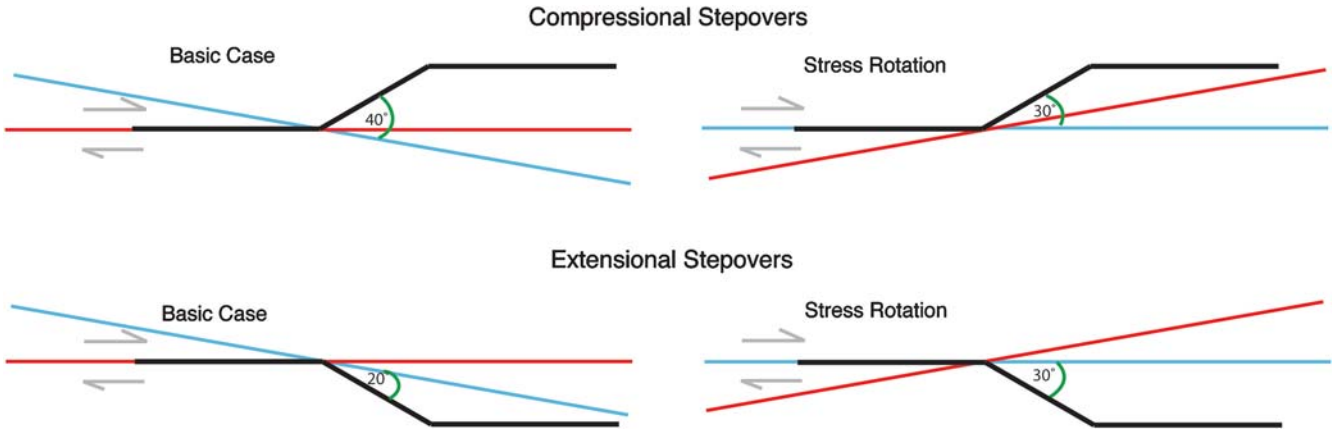

Figure 2. Differences between the regional stress field in the basic case and in the stress rotation case. The fault is shown in black, with gray arrows representing its direction of slip. The red line represents the orientation of maximum shear, and the blue line represents the optimal orientation for rupture (minimum strength excess). All of the stepovers shown in this figure are 30° relative to the parallel end segments; the green arc and the degree measurement represent the angle of the stepover relative to the direction of maximum favorability for rupture. Note that when the parallel end segments are aligned with the direction of maximum shear (basic case), the 30°-compressional stepover is effectively steeper and the 30°-extensional stepover is effectively shallower with respect to the most favorable fault orientation than when the end segments are most favorable for rupture (stress rotation case).

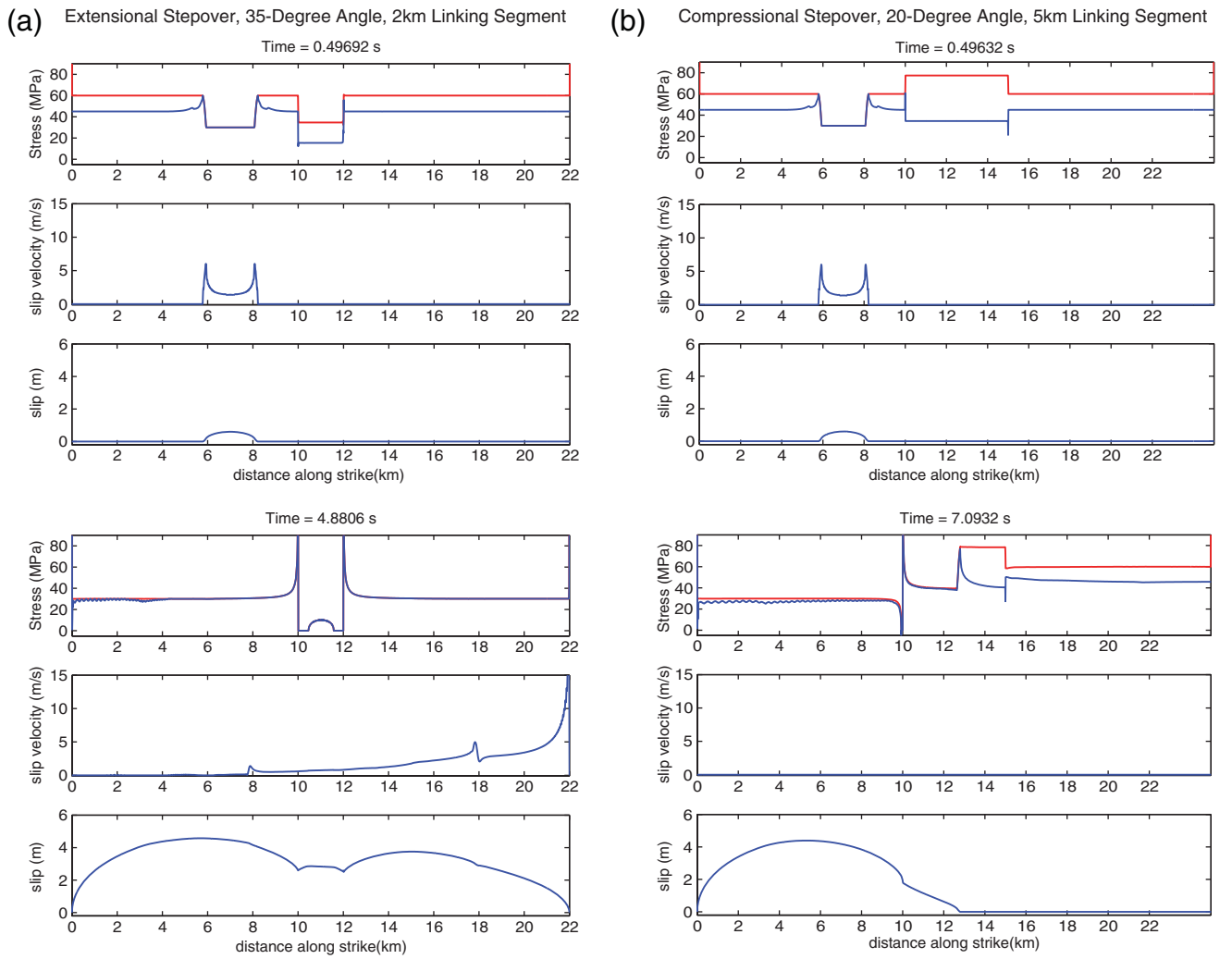

Figure 3. Graphs of rupture behavior. Shear stress in blue, yield stress in red. (a) 35°-extensional stepover with a 2 km linking segment. At 0.4969 s, the rupture behaves as if on a planar fault. By 4.8806 s, the entire fault has ruptured and has started to heal on the nucleating segment; the rest of the fault continues to slip. (b) 20°-compressional stepover with a 5 km linking segment. At 0.49632 s, the rupture behaves as if on a planar fault, exactly as in the extensional case. By 7.0932 s, the fault has stopped slipping and has started to heal, with the rupture front stalled partway through the linking segment. (c) 20°-compressional stepover with a 2 km linking segment. At 0.49632 s, the rupture behaves as if on a planar fault. At 3.3502 s, the rupture has progressed into the stepover and has jumped from the linking segment to the near edge of the far segment. At 3.5621 s, two separate rupture fronts are distinguishable both in the stresses and in the slip rate. (d) 20°-extensional stepover with a 2 km linking segment. At 0.49632 s, the rupture behaves as if on a planar fault. At 0.97196 s, the rupture has jumped from the nucleating segment to the near edge of the linking segment. At 1.0495 s, two separate rupture fronts are distinguishable in both the stresses and the slip rate. (e) 20°-compressional stepover with a 3 km linking segment. By 4.6788 s, the initial rupture has come to a halt in the stepover, and the fault has already healed. Note the small peak in the slip velocity due to a stopping phase from the left end of the fault (circled in green). At 6.3643, the peak in slip velocity reaches the stopping point of the main rupture front, causing it to restart. At 6.478 s, rupture has jumped from the linking segment to the far segment, and two separate rupture fronts are distinguishable in both the slip velocity and the stresses. (*Continued*)

shortly after nucleation. The second graph was created after the completion of rupture, as indicated by the fact that the shear stress and yield stress hold the same value for the entire length of the fault. Parts of the fault are still slipping, and the particularly high peak in slip velocity at the end of the fault indicates a rupture front that has jumped to supershear velocity. In this most basic type of case, which occurred in both extensional and compressional systems, rupture propagated through the entire fault system without stopping, though slowing did occur at the corners of the higher-angle stepovers. In these through-going cases, rupture velocity in the linking segment itself decreased in compressional systems and increased in extensional systems, relative to velocity on the parallel outer segments.

2. Figure 3b includes graphs for rupture on a 20°-compressional stepover with a 5 km linking segment. In the first graph, bilateral rupture progresses in the same way as in the first graph of Figure 3a. In the second graph, rupture has stalled on the stepover segment. The separation of

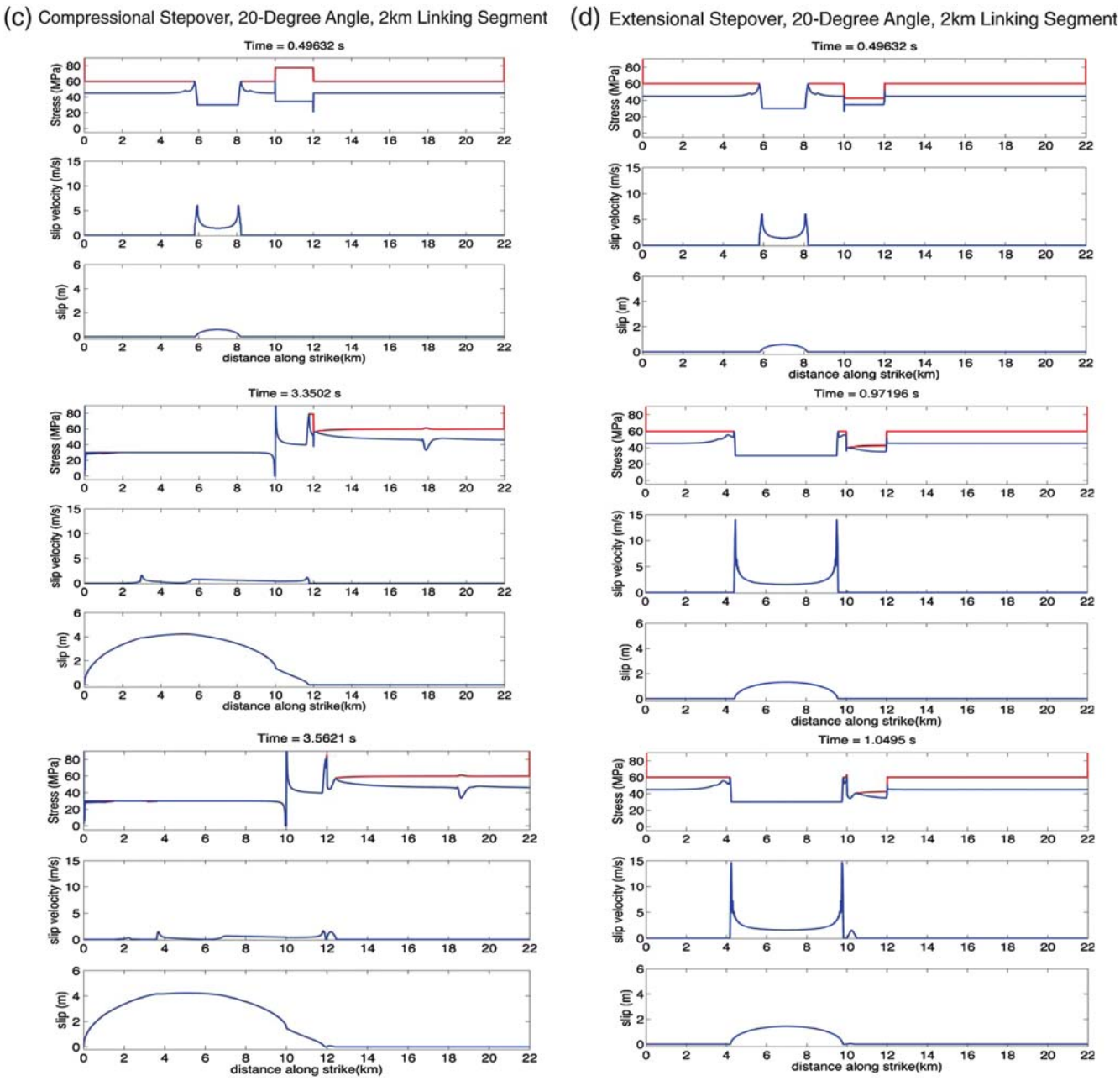

Figure 3. Continued.

yield and shear stresses on the far segment show that it has not ruptured; this is corroborated by the slip velocity being zero, and the total slip for the far segment also being zero. There existed both compressional and extensional cases that were unfavorable enough to stop the rupture from progressing through the entire fault system. This condition was induced either by a particularly steep angle or a particularly long linking segment. In compressional cases, rupture stopped either in the middle of the stepover or at the junction of the nucleating segment and the linking segment. In extensional cases, rupture stopped either in the middle of the stepover or at the junction of the linking segment and the far segment. In both cases, for a given stepover length, steeper angles decreased overall rupture length, with the minimum length being the length of the nucleating segment (10 km). However, as shown below in Figure 4, there were threshold angles and lengths below which rupture propagated through the entire system regardless of the other variable.

3. Figure 3c shows graphs of a 20°-compressional stepover with a 2 km linking segment. The first graph shows that rupture on this fault configuration begins the same way as in Figure 3a,b. However, in compressional systems, rupture sometimes jumped from the less favorable linking segment onto the more favorable right segment of the fault. That is, a second rupture front nucleated on the

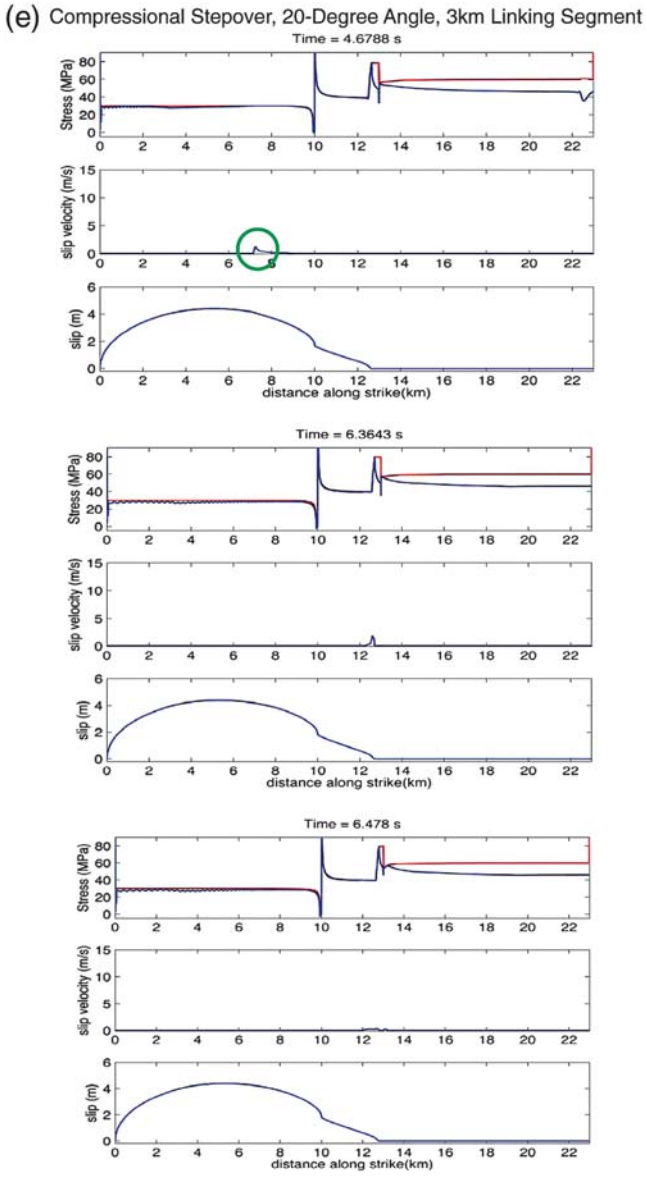

Figure 3. Continued.

right segment, while the main front was still progressing across the linking segment. The second graph in this figure shows the rupture front as it approaches the right corner, and the third graph shows the presence of two separate rupture fronts, as indicated by two peaks in slip velocity, one on either side of the corner. In the majority of cases, the right corner of the stepover did experience slip, either by the continuation of the main rupture front or the bilateral progression of the new front. For all of these cases, once rupture nucleated on the right segment, the entire segment proceeded to rupture. In a very few cases, however, approaching the transition in behavior from rupture of the entire fault to incomplete rupture, a jump occurred but failed to reach the critical patch size necessary to completely rupture the right segment. The end result of these cases was an earthquake that occurred over the left and linking segments of the fault, as well as the first <250 meters of the right segment. A subset of this behavior occurred in systems with steep angles and short stepovers; in these few cases, rupture sometimes jumped directly from the nucleating segment to the far segment, leaving the linking segment untouched.

4. Figure 3d graphs a 20°-extensional stepover with a 2 km linking segment. Extensional systems such as this one also exhibited jumping rupture. The first graph shows that these ruptures nucleate in the same way as all the other cases shown thus far. In this case, however, rupture jumps from the nucleating segment to the linking segment. The second graph shows the initial rupture front approaching this corner. The third graph was taken after

the jump; the second rupture front is distinguishable as a peak in slip velocity to the right of the corner. The junction between the nucleating segment and the linking segment always experienced slip, and critical patch size on the linking segment was always reached, as unclamping makes extensional cases more dynamically favorable for rupture. Rupture did not necessarily reach the right corner in all extensional cases, as static unfavorability (due to misalignment of the linking fault with the static stress field) outweighed dynamic favorability for steeper angles and longer lengths.

5. Figure 3e shows graphs of rupture on a 20°-compressional stepover with a 3 km linking segment. They highlight a final characteristic behavior that occurred in both extensional and compressional cases, in systems where the main rupture front stopped propagating within a very short distance of the next segment, leaving the shear stress quite close to the yield stress. When the bilateral rupture on the nucleating segment hit the left edge of that segment, a small stopping phase wave propagated rightward back along the fault. This phase, which manifests as a small peak in slip velocity, is circled in green in the first graph. When this phase reached a stalled rupture front as described previously, it was sometimes energetic enough to restart the rupture after a lag time of several seconds. The second graph shows the stopping phase approaching the stalled rupture front; note how it has intensified relative to the first graph. In compressional cases, this meant initiating a jump from the linking segment to the far segment, as indicated by the two peaks in slip velocity in the third graph; in most of these cases, the rupture proceeded down the rest of the far segment, but in some, critical patch size was not reached on the far segment after the jump, and the rupture stopped again. In extensional cases, the stopping phase wave caused stalled rupture fronts to proceed from the linking segment to the far segment without any jumping.

The results of this parameterization are displayed in Figure 4. These are plots of the length of the linking segment versus the stepover angle, for both compressional and extensional cases. Each symbol represents a single model and is color-coded depending on the rupture behaviors described in Figure 3. Both plots show distinct regions of rupture behavior in stepover angle-linking segment length space. The shallower the stepover angle, the less of an effect the length of the linking segment had on rupture propagation. For extensional cases (Fig. 4a), stepovers with angles of less than 34° will always fully rupture, regardless of the length of the linking segment; in compressional cases (Fig. 4b), angles of less than 18° do not inhibit rupture. This highlights one key result of this study: that, for these stress assumptions, extensional stepovers will rupture through a wider range of angles than compressional stepovers will. Unsurprisingly, the shorter the linking segment, the less of an effect the stepover angle has on rupture propagation. In the extensional and compressional cases with the shortest linking segments (500 m), no stepover angle was steep enough to inhibit rupture propagation (though, in the steepest compressional cases, rupture jumped from the nucleating segment to the far segment without rupturing the linking segment). For linking segments longer than 500 m and stepover angles larger than the threshold in both extensional and compressional cases, both variables participate in controlling rupture behavior.

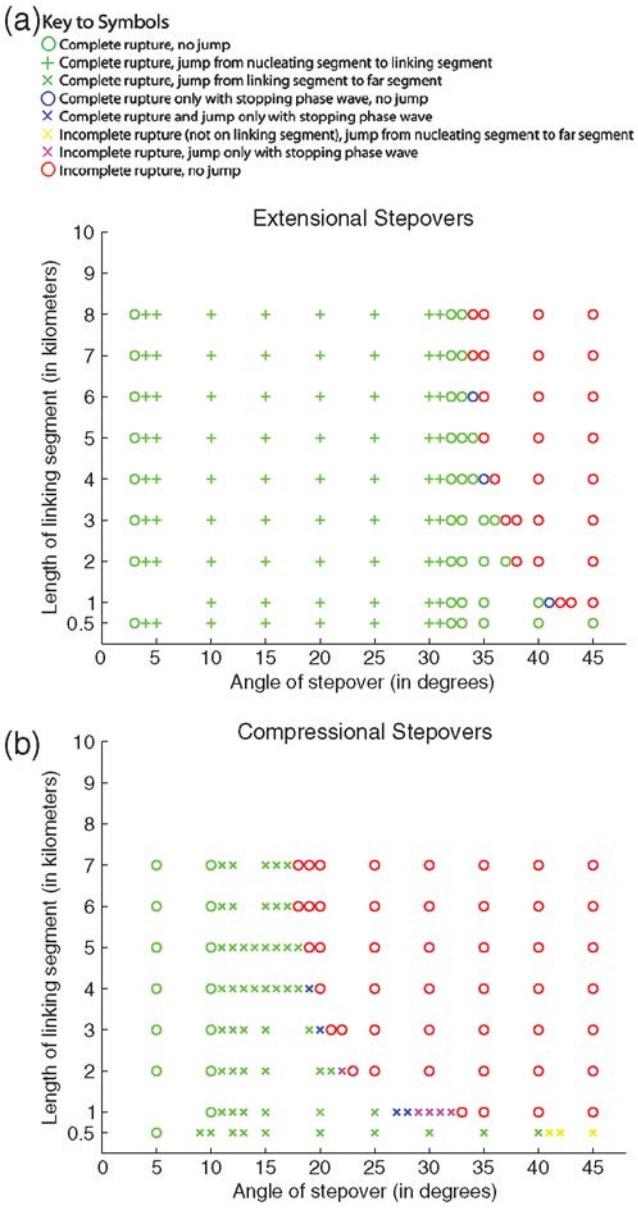

Figure 4. Parameterization charts for rupture behavior in basic case extensional and compressional stepovers. Each symbol represents one numerical model. Note that both the angle and the width of stepover affect rupture behavior. Both small angles and short stepover lengths facilitate full propagation. Also note the asymptotic curve marking the boundary between different behaviors on both charts.

There is a clear dependence on whether rupture progresses smoothly or whether it jumps from segment to

segment on stepover angle. In compressional cases, stepover angles of between 10° and the angle that ultimately stops rupture for that given linking segment length induced jumping rupture. In extensional cases, systems with a stepover angle between 4° and 31° exhibit jumping rupture, regardless of the length of the linking segment. Restarting of stalled rupture fronts by the passing of a stopping phase occurs as a transitional behavior; restarted rupture may happen for stepover angles of several degrees shallower than the angle at which rupture is stopped for a given linking segment length. Restarted rupture was more prevalent in compressional stepovers than in extensional ones.

Scaling Test

Fault systems of different sizes will tend to experience different rupture velocities and different sizes of the process zone around the crack tip. To investigate such scale differences in our models, we performed models in which the entire fault system was made larger or smaller in size relative to our basic case (as opposed to simply varying the length of the linking segment relative to the parallel end segments). The scaling affected the lengths of the fault segments, but aspects such as slip-weakening parameter and critical patch size remained the same as in the basic case. Element size was also fixed at 10 m. In order to isolate the effects of rupture velocity on the results, we ran two sets of scaling tests: one with the nucleation coordinate scaled up or down with the system (i.e., at 6 km from the right edge of the nucleating segment in a system twice as big as the initial case), and one with the nucleation point held fixed at 3 km from the left-most bend. In the models where the nucleation point scales with overall system size, the velocity of the rupture front changes with the distance from the nucleation point to the junction of the nucleating segment and the linking segment. In contrast, the rupture velocity remains constant at this junction if all ruptures nucleate at 3 km from the corner, regardless of system size. For the scaled nucleation set, we ran systems 1/4, 1/2, and 2 times the scale of the original; for fixed nucleation, we could not do the 1/4 size case because the parallel end segments were only 2.5 km long, which did not allow a nucleation point 3 km from the left corner. Figure 5 shows a diagram of these different system sizes and nucleation point cases. Rather than running a full spectrum of stepover lengths and angles as we did in the basic case, we selected a representative angle (20° for compressional and 35° for extensional) that included a wide range of rupture behaviors, then modeled stepovers of different lengths at that one angle.

The results for both scaling tests in both compressional and extensional cases are shown in Figure 6. The x axis indicates the length of the parallel end segments in the model relative to the length of the parallel end segments in the basic case (10 km each). The y axis indicates the length of the linking segment relative to the length of one of the parallel end segments. Each symbol represents a single model, color-coded to show rupture behavior as in Figure 4.

These results clearly indicate that rupture behavior does not scale linearly with overall fault system size. Larger-scale fault systems were more likely to rupture fully than smaller-scale ones, even with linking segments that were long relative to the length of the parallel end segments (i.e., a fault with 20 km parallel end segments and a 14 km linking segment). The full range of rupture behaviors (jumping, stopping phase restart, incomplete rupture) was still exhibited in both upscaled and downscaled fault systems. Differences between the scaled nucleation cases and the fixed nucleation cases were negligible, and generally involved stopping phase restarts, suggesting that rupture velocity (at least at the first bend) does not have a strong influence on the scaled results. All of these effects are likely more pronounced due to our use of 2D models; in a 3D fault, the depth of the seismogenic zone may provide a constraint that saturates out some of the effects of the length scale of the fault system.

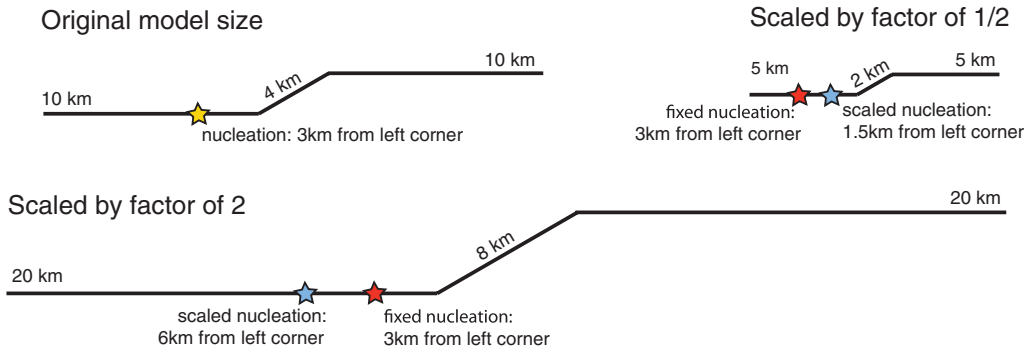

Figure 5. Different scales of a stepover system. The original model size, as in all of the models in the basic case, is shown on the upper left. A 1/2-sized model is on the upper right, and a model scaled up by a factor of 2 is on the bottom. In the scaled systems, both the length of the parallel end segments and the length of the linking segment change. In the original model, the nucleation point is marked with a yellow star. In the scaled models, the red star represents a fixed nucleation point at 3 km from the junction of the nucleating segment and the linking segment. The blue star represents a nucleation point that scales left or right with the overall system size.

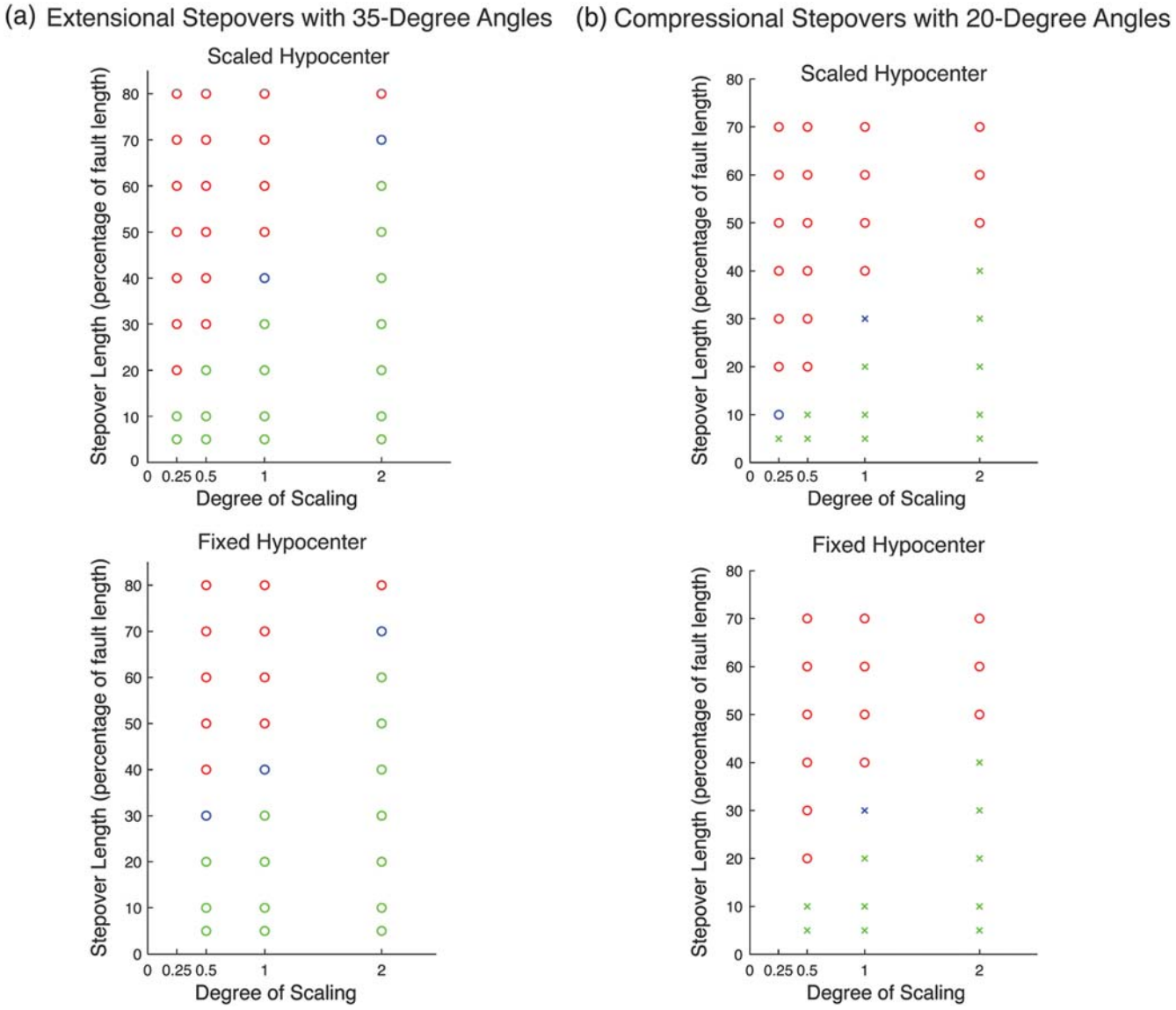

Figure 6. Results of scaling tests for extensional and compressional stepovers with (a) 35° and (b) 20° angles. Note that whether the nucleation point was scaled or fixed has negligible effect on rupture behavior in both stepover types. Also note that rupture propagated through proportionally larger stepovers in fault systems that were larger overall. Each symbol represents one model; the key to symbols is the same as for Figure 4.

Stress Rotation

The stress field in the basic case and the scaled cases is such that the parallel end segments are aligned with the direction of maximum shear stress. This is a plausible configuration for faults in the field, but at least equally plausible is an alignment in which the parallel end segments are optimally oriented for rupture. In order to replicate this situation in our models, we interpreted optimally oriented as a minimization of strength excess over the fault in a given regional stress field. A comparison of the stress values between the basic case and the stress rotation case is in Table 2. Note that the shear and normal stresses on the main fault segments are equal to our previous case; it is the shear and normal stresses on the linking faults that change.

As in the basic case, the parallel end segments of the fault were fixed at 10 km each, with nucleation at 3 km from the corner of the nucleating segment and the linking segment. We performed a range of models with different lengths of linking segment over a range of angles up to 45°, though in this case, we were only concerned with whether the fault

Table 2
Regional Stresses

Stress Case	Basic Case	Stress Rotation Case
East–west normal stress	−100 MPa	−154 MPa
North–south normal stress	−100 MPa	−100 MPa
Shear stress	45 MPa	45 MPa

fully ruptures, as opposed to the transitions between the other rupture behaviors identified earlier.

Results for the stress rotation case are shown in Figure 7. As in Figure 4, these are plots of linking segment length versus stepover angle. Each symbol represents a single model and uses the same color-code to indicate rupture behavior as in Figure 4. In this case, we were interested in tracking the stepover angles and linking segment lengths that stop rupture propagation. Under the assumption that the overall shapes of the result plots (but not the specific values) would be comparable to those in the basic case, we did not feel that we needed to fill in the rest of parameter space on either side of the behavior transition curve.

As in the basic case, both extensional and compressional cases had threshold angles below which rupture would always propagate through the entire fault system, regardless of linking segment length. The general shapes of the results curves in parameter space were similar between the stress rotation case and the basic case, but the angles were significantly shifted from in the basic case. For extensional cases (Fig. 7a), the entire fault ruptured if the stepover angle was less than 18° (as opposed to 34° in the basic case). For compressional cases (Fig. 7b), angles shallower than 31° guaranteed full rupture propagation (as opposed to 18° in the basic case). The effect of linking segment length on rupture propagation in the stress rotation case is greater for extensional stepovers than for compressional ones. In the extensional case, linking segment lengths of up to 9 km still influence rupture propagation; in the compressional case, linking segment lengths of 4 km and longer make no difference in rupture behavior. The ability of rupture to progress through the entire fault regardless of angle for stepover segments of 500 m was consistent between the basic case and the stress rotation case for compressional systems; for extensional systems, there was no linking segment length short enough to guarantee full rupture regardless of stepover angle.

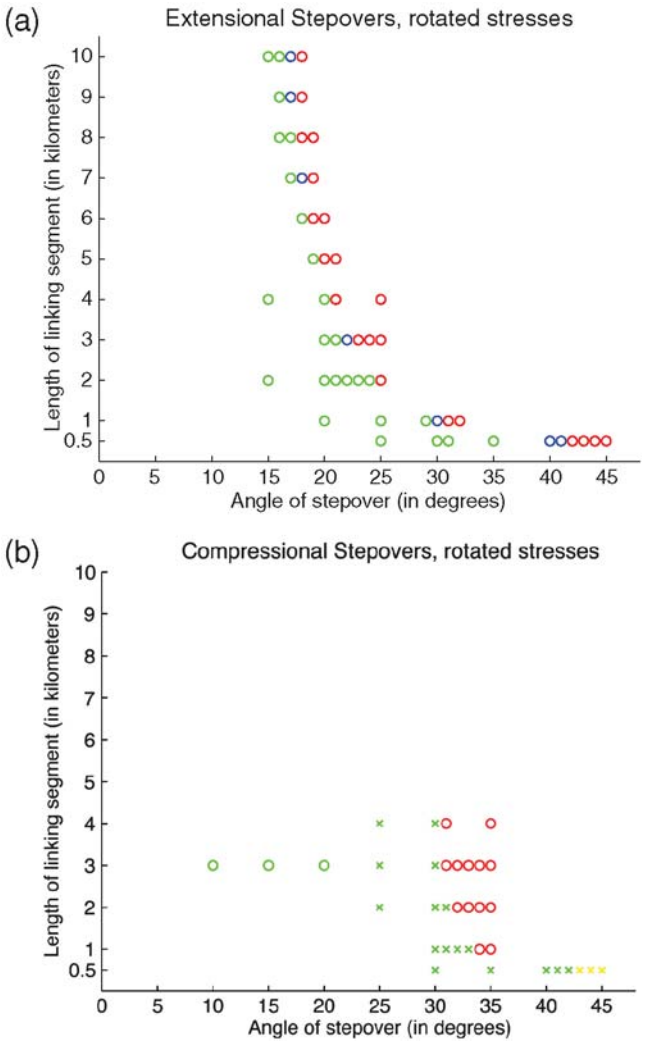

Figure 7. Parameterization of rupture behavior for (a) extensional stresses and (b) compressional stepovers with parallel end segments aligned most optimally for rupture. Note that compressional stepovers are easier to rupture than extensional ones are, opposite to the basic case. Also note that asymptotic behavior manifests itself at a much shorter linking segment length for compressional stepovers than for extensional ones. Each symbol represents one numerical model; the key to symbols is the same as in Figure 4.

We observed no jumping rupture in the extensional cases that we modeled for the stress rotation case, but it is still possible that jumping rupture occurs for angles shallower than the ones investigated here. In compressional cases, jumping rupture occurs in systems of a stepover angle of greater than 20° and less than the angle at which rupture was halted for that given linking segment length. There are no instances of a stopping phase restarting a stalled rupture front in the compressional case; in the extensional case, jumping rupture may occur for stepover angles a few degrees shallower than the angle at which rupture is halted for a given linking segment length.

Discussion

Basic Case

One of our key findings is that, for a stress field in which the primary fault segments are aligned with the direction of maximum shear, a rupture front can proceed through a wider stepover for a given stepover angle in an extensional case than for the same angle in a compressional one. This result is generally consistent with the results of previous studies (Harris and Day, 1993) on unlinked stepovers. The maximum distances able to be propagated through in both extensional and compressional cases were considerably larger than distances determined for unlinked stepovers (Harris and Day, 1993; Oglesby, 2008), which brings our results in line with other studies that found that rupture can traverse longer stepover distances when a linking segment is present (Magistrale and Day, 1999; Oglesby, 2005).

In the case of main segments aligned with maximum shear, the rupture behavior curves for both extensional and compressional stepovers can be explained by the balance between static and dynamic effects. Dynamic clamping of

the linking segment in compressional stepovers makes it more difficult for rupture to propagate through to the other main fault segment. In compressional cases, all stepover angles are also statically less favorable for rupture than the main segments. The combination of static and dynamic unfavorability in compressional cases explains why the threshold falls at a shallower angle and shorter stepover length than in extensional cases (i.e., there is a smaller region of parameter space that allows through-going rupture in the compressional case). In extensional cases, dynamic unclamping of the linking segment reduces normal stress and makes it easier for rupture to propagate through to the far segment within a certain range of angles. For successively steeper stepover angles, the fault becomes so unclamped that there is not enough static shear stress resolved on the linking fault for a rupture front to be maintained. The static stress associated with extensional stepovers is also more complicated, as the angle at which a fault segment is most favorable for rupture falls within the range of angles for extensional stepovers. Thus, some linking segments in extensional cases are more statically favorable for rupture than the parallel end segments of the fault. Beyond this angle, extensional linking segments become statically unfavorable as well. As extensional stepovers transition between being dynamically favorable and unfavorable, as well as statically favorable and unfavorable, they are a more complex case than compressional stepovers in this stress configuration. The combination of favorable dynamics and statics explains why the threshold in extensional cases falls at a much steeper angle than in compressional cases, as well as at a longer linking segment length.

Figure 8 shows the regional prestress field, stress drop, and relative fault strength S for the basic case resolved onto linking faults at a variety of orientations. Compressional stepovers are shown as positive angles and extensional ones as negative. The fault's S value ($S = \frac{\sigma_y - \sigma_0}{\sigma_0 - \sigma_f}$, where σ_y is the fault's yield stress, σ_0 is the initial shear stress, and $\sigma_0 - \sigma_f$ is the dynamic stress drop) is a representation of how close the fault is to failure under the initial stress field (Das and Aki, 1977). It is represented on the figure by the green curve, and it diverges at 18° on the compressional side and at 34° on the extensional side (angles at which the stress drop changes sign), which aligns exactly with the threshold angles we found in our exploration of parameter space. This result implies that these peaks in S determine the maximum angle at which rupture can propagate across an arbitrarily long linking fault; it corresponds to the largest angle for which the static stress field is favorable for rupture. This correlation of the prestresses with the threshold angle also suggests that, for longer fault systems, the static prestress effect dominates over the effects of dynamics and fault interaction to determine rupture behavior. Dynamic interactions between fault segments at the corners allows rupture to progress through steeper angles when the linking segment is short; once the linking segment becomes long enough to prevent significant normal stress modification over a significant portion of the linking fault, the static effect dominates. This finding is consistent with work done by Aochi *et al.* (2002) on branching fault systems and with work on faults with simple bends conducted by Kase and Day (2006).

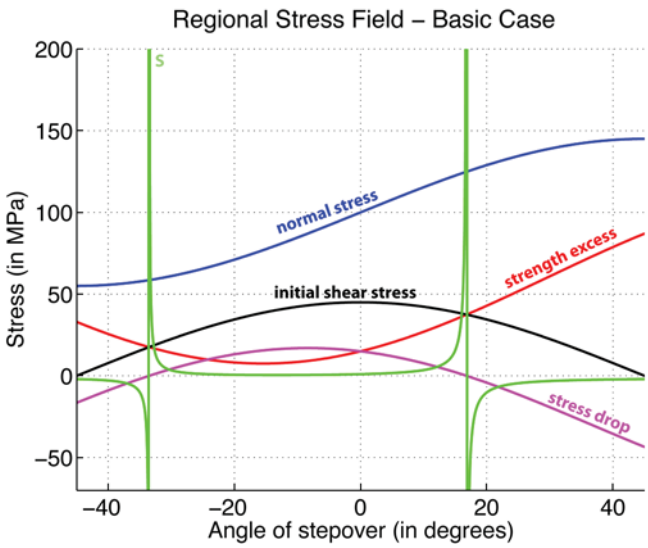

Figure 8. Regional stress field resolved onto the linking fault for the basic case, in which the parallel end segments of the fault are aligned with the direction of maximum shear. Angles above 0 represent compressional stepovers, and angles below 0 represent extensional stepovers. The blue line represents the absolute value of normal stress; the black line represents initial shear stress; and the red curve represents strength excess on the fault, defined as the difference between yield stress and initial shear stress. Relative fault strength S is shown in green; stress drop is shown in magenta. Note that the peaks in S occur at the same angles as the thresholds below which the entire fault always ruptures in Figure 4.

The stopping phase wave that is produced when the initial rupture front reaches the left terminus of the nucleating segment has not been described in any prior study, although it may well have been present. We believe that it is a real effect within the parameters of our model, but that it is not likely to occur in the real world. In our slip-weakening models, the fault does not heal after the main rupture front passes it, so a small stress perturbation could be enough to restart rupture. Laboratory studies (e.g., Dieterich, 1979) imply that this behavior may be unrealistic; the section of fault that ruptured early in a large earthquake may be healed before the earthquake has run its course on other parts of the fault. A pulse the size of the stopping phase observed in our models would likely not be strong enough to restart rupture on a fault that had already begun to heal. As all of the cases within this study that exhibited this behavior were clustered around the transition point between whether or not the entire fault ruptured, they affect the shape of the rupture behavior curve, particularly for shorter stepover lengths, but not the final location of the threshold.

Scaling Test

When we altered the scale of the entire fault system, rather than just varying the length of the stepover segment,

we found that rupture behavior transitions did not scale linearly with the size of the entire fault system. In other words, doubling the size of the system did not result in doubling the maximum stepover length. Rather, we found that rupture was more likely to propagate through proportionately larger stepover segments when the entire system scale was larger than in the basic case, and that it was more likely to be stopped by proportionately smaller stepovers if the whole system was smaller. Running tests with both fixed nucleation points and nucleation points scaled relative to overall system scale ruled out rupture velocity (at least at the left corner) as the cause of this nonlinear relationship. This is likely at least partly an effect of the slip-weakening parameter, which we did not scale up or down with the rest of the system. For a larger fault, the same slip-weakening parameter is effectively shorter compared to the fault length than in a smaller fault. This faster weakening creates a more energetic rupture front that is capable of propagating over a longer relative distance. These effects may, however, be exaggerated by our use of 2D models. The depth of the seismogenic zone is not a factor in 2D models, but in a 3D model, or in the real world, the depth of this zone is a constraint that may cause length scale effects to saturate. We examined a representative angle for each stepover type, rather than producing a full parameterization curve at each system size, so we did not determine how overall fault system size affects the shape and placement of the asymptotic rupture behavior curve.

Stress Rotation

Our initial hypothesis regarding the stress rotation models was that the behavior curves for extensional and compressional cases would become more like each other in terms of steepness of the asymptotic curve, and in terms of angle at which rupture no longer propagated through the stepover. Our reasoning was that if the parallel end segments were set as being most favorable for rupture, a stepover at any angle would be inherently less favorable, regardless of stepover type.

The results we found from these simulations are more counterintuitive. In this stress configuration, compressional stepovers are actually easier to rupture at steeper angles than extensional stepovers are; this is the opposite of the case in which the parallel end segments are aligned with the direction of maximum shear. This can be largely explained by a decrease in static favorability in the extensional cases.

For successively steeper stepover angles in the extensional case, the stress drop approaches zero, which is not conducive to supporting a propagating rupture front; this effect prevented full propagation through steep extensional stepovers in the basic case as well. Because the most favorable stepover angle is 0° in the rotated stress case, all extensional stepover angles are statically less favorable for rupture than the equivalent angles in the basic case. For steeper and steeper stepover angles, the linking segment becomes more extended and unclamped. Both the normal stress and the shear stress become extremely low, to the point where the stress drop across the stepover segment may actually be negative. This does not allow for the buildup of enough elastic energy to maintain a rupture front across the entire stepover segment. Our findings that the orientation of the regional stress field controls rupture favorability (at least for long linking faults) more than dynamic stress changes do agrees with past work on this issue (Aochi *et al.*, 2002). The delineation of the transition between the dominance of dynamic and static effects, though, is an important new result.

In the rotated compressional cases, larger angles can be propagated through than in the basic case. Figure 2 explains this effect graphically. When the end segments of the fault (shown in black) are aligned with the direction of maximum shear (shown in red), compressional stepovers are less statically favorable than extensional ones, as the most favorable angle for rupture (shown in blue) falls within the realm of extensional stepovers. By aligning the end segments with that most favorable angle, steeper compressional stepover angles are made effectively shallower with respect to the regional stress field, and therefore more favorable for rupture themselves.

At certain cutoff angles, the stress rotations may impose the situation in which the direction of shear on the linking segment becomes the reverse of the direction of shear on the parallel end segments (i.e., a left-lateral stepover segment linking two right-lateral end segments). This is a situation that is unlikely to occur in nature, but we ran models for these situations anyway for the sake of thoroughness of parameterization. The unnatural setup of these faults manifested in the results curves. The angle at which the direction of shear on the stepover segment switched in the extensional cases was 30°. Rupture could not propagate all the way through extensional stepovers of 30° or steeper in all but the 1 km and 500 m linking segment cases, and full rupture only occurred after a stopping phase restart in the 1 km case. The cutoff angle in compressional cases was 30° in the other direction. Thirty degrees was the steepest angle through which rupture could fully propagate in compressional cases; the fact that it was reached at relatively short stepover lengths explains why we did not have to run models of longer stepovers in order to find the asymptote.

Figure 9 shows the regional prestress field for the stress rotation case. The strength excess is represented by the red line. The point at which it is minimized, thus defining the fault alignment that is most favorable for rupture, is centered at 0° on this chart, with compressional stepovers being positive angles and extensional stepovers being negative. The green line represents *S*, and as in the basic case, it makes sharp peaks at angles corresponding with the asymptotes revealed in the parameter study: 30° for compressional stepovers, 16° for extensional. The stress drop is represented by the magenta line, and it becomes negative at the same angles as the peaks in *S*, also corresponding with the angle at which rupture will no longer propagate through the entire fault

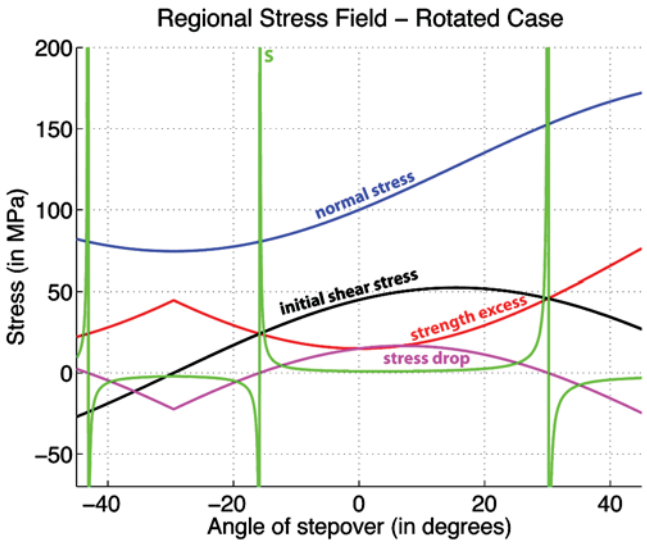

Figure 9. Regional stress field resolved onto the linking fault for the stress rotated case, in which the parallel end segments of the fault system are optimally aligned for rupture, as determined by minimization of the fault's strength excess. Angles above 0 represent compressional stepovers, and angles below 0 represent extensional stepovers. The blue line represents the absolute value of normal stress; the black line represents initial shear stress; and the red curve represents strength excess on the fault, defined as the difference between yield stress and initial shear stress. Relative fault strength *S* is shown in green; stress drop is shown in magenta. Note that the peaks in strength excess are shifted from the basic case (Fig. 8), and that they align with the asymptotes in Figure 7.

system. As in the basic case, the stress rotation results reveal that, as the fault becomes longer, rupture behavior transitions from being governed by interactions between different fault segments to being controlled by the regional prestress field.

Comparison with Historical Rupture Data

Our model results can be discussed along with the data on historical surface ruptures collected by Wesnousky (2008). Seventy percent of the 46 strike-slip ruptures in his study terminated either at geometrical complexity along strike or at the end of the mapped fault trace. He also notes that, for faults with mapped disconnected stepovers, rupture did not propagate through discontinuities of more than 3–4 km in any of the historical cases in the study, and that rupture propagated through smaller discontinuities only 40% of the time. Within this, historical ruptures traversed wider extensional steps than compressional ones.

A completely parallel comparison cannot be made between these field data and our model results because our models are simplified as to isolate one major effect, and because precise source characteristics are not known for some of the older ruptures in Wesnousky's study. However, both this field data and our model data strongly support the statement that geometrical discontinuities along fault traces can serve as significant impediments or endpoints for rupture. In our models, rupture was able to propagate through wider discontinuities than in Wesnousky's study, but as discussed previously, rupture does not need to renucleate in order to traverse a linked stepover, and can therefore proceed through wider discontinuities. The historical ruptures in Wesnousky's study were likely in a wide variety of different regional stress field orientations, but the fact that all the ruptures in question stopped at discontinuities of 3 to 4 km places them within the region of parameter space in the present study in which dynamic clamping and unclamping control propagation more than static favorability does. In this situation, it makes sense that rupture would consistently be able to proceed through wider extensional stepovers than compressional ones.

Summary and Conclusions

For strike-slip faults with stepovers linked by strike-slip segments in a stress regime in which the parallel end segments are aligned with the direction of maximum shear, there is a threshold angle below which rupture will always propagate through the entire fault regardless of linking segment length (18° for compressional, 24° for extensional); there is also a linking segment length at which rupture will always propagate through the entire fault regardless of stepover angle (500 m for both extensional and compressional). For steeper stepover angles and longer linking segments, both stepover angle and linking segment length contribute to rupture behavior. This result is a function of the balance between static and dynamic favorability in both cases. In some cases that were on the borderline between whether or not the rupture propagated through the entire fault, a stopping phase wave from the end of the fault was able to restart the rupture. While this behavior was a significant feature of our models, it likely does not occur in the real world.

Scaling the entire fault system up or down suggested that it was easier to propagate rupture through a proportionately larger stepover in fault systems that were overall larger in scale. Longer fault systems with stepovers are more likely to rupture fully despite the geometrical continuities. Geometrical discontinuities are more of a rupture barrier in shorter faults than in longer ones. This behavior is likely related to the length of the slip-weakening parameter relative to the size of the fault, with smaller slip-weakening parameters leaving more energy available for the rupture front. We did not test the effects of scaling the slip-weakening parameter with the rest of the system.

Rotating the regional stress field so that the parallel end segments of the fault system were optimally aligned for rupture produced the counterintuitive result that compressional stepovers were easier to fully rupture than extensional ones were. The decreased favorability of extensional stepovers comes from an extreme decrease in stress drop on the linking segment, so that a rupture front cannot be maintained across it. The steeper propagation angles of compressional stepovers are due to improved static favorability in this stress case. These results suggest that the alignment of the regional

stress field makes a significant difference in how both extensional and compressional stepovers behave. Furthermore, the idea of a regional stress field is an approximation; stresses surrounding real world faults may diverge from the overall regional field, or may be heterogeneous even along individual faults due to long-term stress interactions between fault segments (Duan and Oglesby, 2006) as well as dynamically induced heterogeneities.

The implications of this result are somewhat daunting: because we do not know the orientation of stresses in the crust very precisely or at high resolution, it is difficult to estimate rupture length and behavior. However, our results still do suggest that, regardless of regional stress field, extensional and compressional stepovers behave differently from each other. Our results reaffirm past studies describing dynamic clamping and unclamping of compressional and extensional stepovers respectively (Oglesby, 2005). Our results also still allow for some projection of where along the fault trace a rupture might die out based on stepover type, which still allows for some estimation of magnitude. The fact that the peaks in S imposed by the static stress field predict quite well the threshold angles at which rupture will no longer propagate through the entire fault implies that, for faults with shorter linking segments, the interaction between fault segments controls rupture behavior, but that static prestress effects dominate behavior for faults with longer linking segments.

Data and Resources

No external data were used in this paper. All results were generated using EQdyna2d (Duan and Oglesby, 2006), and all figures were generated using either MATLAB or Adobe Illustrator.

Acknowledgments

The authors thank Ruth Harris, Steven Day, Yuko Kase, and Elizabeth Templeton-Barrett for useful conversations concerning this work. This research was supported by the Southern California Earthquake Center. SCEC is funded by NSF Cooperative Agreement EAR-0106924 and USGS Cooperative Agreement 02HQAG0008.

References

Anderson, G., B. Aagaard, and K. Hudnut (2003). Fault interactions and large complex earthquakes in the Los Angeles area, *Science* **302,** 1946–1949.

Andrews, D. J. (1976a). Rupture propagation with finite stress in antiplane strain, *J. Geophys. Res.* **81,** 3575–3582.

Andrews, D. J. (1976b). Rupture velocity of plane strane shear cracks, *J. Geophys. Res.* **81,** 5679–5687.

Aochi, H., E. Fukuyama, and M. Matsu'ura (2000). Spontaneous rupture propagation on a non-planar fault in 3-D elastic medium, *Pure Appl. Geophys.* **157,** 2003–2027.

Aochi, H., R. Madariaga, and E. Fukuyama (2002). Effects of normal stress during rupture propagation along nonplanar faults, *J. Geophys. Res.* **107,** doi 10.1029/2001JB000500.

Das, S., and K. Aki (1977). A numerical study of two-dimensional spontaneous rupture propagation, *Geophys. J. R. Astr. Soc.* **50,** 643–668.

Day, S. M. (1982). Three-dimensional simulation of spontaneous rupture: The effect of nonuniform prestress, *Bull. Seismol. Soc. Am.* **72,** 1881–1902.

Dieterich, J. H. (1979). Modeling of rock friction, 1, Experimental results and constitutive equations, *J. Geophys. Res.* **84,** 2161–2168.

Duan, B., and D. D. Oglesby (2005). Multicycle dynamics of nonplanar strike-slip faults, *J. Geophys. Res.* **110,** doi 10.1029/2004JB003298.

Duan, B., and D. D. Oglesby (2006). Heterogeneous fault stresses from previous earthquakes and the effect on the dynamics of parallel strike-slip faults, *J. Geophys. Res.* **111,** B05309, doi 10.1029/2005JB004138.

Duan, B., and D. D. Oglesby (2007). Nonuniform prestress from prior earthquakes and the effect on dynamics on branched fault systems, *J. Geophys. Res.* **112,** B05308, doi 10.1029/2006JB004443.

Harris, R. A., and S. M. Day (1993). Dynamics of fault interaction: Parallel strike-slip faults, *J. Geophys. Res.* **98,** 4461–4472.

Harris, R. A., R. J. Archuleta, and S. M. Day (1991). Fault steps and the dynamic rupture process—2-D numerical simulations of a spontaneously propagating shear fracture, *Geophys. Res. Lett.* **18,** 893–896.

Ida, Y. (1972). Cohesive force across the tip of a longitudinal shear crack and Griffith's specific surface energy, *J. Geophys. Res.* **77,** 3796–3805.

Kame, N., J. R. Rice, and R. Dmowska (2003). Effects of pre-stress state and rupture velocity on dynamic fault branching, *J. Geophys. Res.* **108,** no. 2265, doi 10.1029/2002JB002189.

Kase, Y., and S. M. Day (2006). Spontaneous rupture processes on a bending fault, *Geophys. Res. Lett.* **33,** doi 10.1029/2006GL025870.

Magistrale, H., and S. M. Day (1999). 3D simulations of multi-segment thrust fault rupture, *Geophys. Res. Lett.* **26,** 2093–2096.

Oglesby, D. D. (2005). The dynamics of strike-slip step-overs with linking dip-slip faults, *Bull. Seismol. Soc. Am.* **95,** 1604–1622.

Oglesby, D. D. (2008). Rupture termination and jump on parallel offset faults, *Bull. Seismol. Soc. Am.* **98,** 440–447.

Oglesby, D. D., S. M. Day, Y.-G. Li, and J. E. Vidale (2003). The 1999 Hector Mine earthquake: The dynamics of a branched fault system, *Bull. Seismol. Soc. Am.* **93,** 2459–2476.

Palmer, A. C., and J. R. Rice (1973). The growth of slip surfaces in the progressive failure of overconsolidated clay, *Proc. of the Royal Society of London Series A* **332,** 527–548.

Segall, P., and D. D. Pollard (1980). Mechanics of discontinuous faults, *J. Geophys. Res.* **85,** 4337–4350.

Wesnousky, S. G. (2008). Displacement and geometrical characteristics of earthquake surface ruptures: Issues and implications for seismic-hazard analysis and the process of earthquake rupture, *Bull. Seismol. Soc. Am.* **98,** 1609–1632.

Department of Earth Sciences
University of California, Riverside
Riverside, California 92521
jlozo001@ucr.edu
david.oglesby@ucr.edu
(J.C.L., D.D.O.)

Center for Tectonophysics
Department of Geology and Geophysics
Texas A & M University
College Station, Texas 77843
duan@geo.tamu.edu
(B.D.)

Center for Neotectonic Studies
University of Nevada
Reno Mail Stop 169
Reno, Nevada 89557
stevew@seismo.unr.edu
(S.G.W.)

Manuscript received 26 January 2010